

Theoretical performance characteristics of a travelling-wave phase-change thermoacoustic heat pump

Rui Yang^{a,b}, Nathan Blanc^c, Guy Z. Ramon^{c,*}

^a CAS Key Laboratory of Cryogenics, Technical Institute of Physics and Chemistry, Chinese Academy of Sciences, Beijing 100190, China

^b Department of Civil & Environmental Engineering, Technion – Israel Institute of Technology, Haifa 32000, Israel

^c The Nancy and Stephen Grand Technion Energy Program, Technion – Israel Institute of Technology, Haifa 32000, Israel

ARTICLE INFO

Keywords:

Thermoacoustic refrigerator
Thermoacoustic heat pump
Phase change
Wet thermoacoustics
Travelling wave

ABSTRACT

Thermoacoustic technology is a promising approach for environmentally-benign, low-cost heat pumping. Herein, we present a theoretical investigation on phase-change thermoacoustic heat pumping employing both an ideal model (a short heat pump in a pure travelling-wave field), as well as a full-size, looped-tube thermoacoustic heat pump. In the analysis of the short heat pump, we identified and assessed the main factors and their influence on the performance of an ideal phase-change travelling-wave heat pump. The results show that, ideally, the cooling power can be significantly increased by up to one order of magnitude, and the *COP* (coefficient of performance) can also be improved by the incorporation of phase change into the thermoacoustic cycle. Meanwhile, the analysis of the full system provides a more practical view of the enhancement due to phase change. A significant increase of cooling power is observed in the phase-change system with a high concentration of the reactive component, but increased of the *COP* only occurs under small temperature differences (below 10 K). The main reason for the gap in observed performance between the ideal model and the full system is the deviation, under a large temperature difference, of the acoustic field from the requirements for effective enhancement, as revealed in the ideal model. Our results demonstrate the potential of the phase-change travelling-wave thermoacoustic heat pump for efficient and low-cost heat pumping, especially for small temperature difference applications.

1. Introduction

It is estimated that, by the end of the century, the demand for global air conditioning would grow by as much as 83%, leading to a potential increase of up to 23 million tons of annual carbon dioxide emissions [1]. Therefore, developing environmentally-friendly heat pumping technologies with high efficiency and low costs is an urgent issue [2].

The thermoacoustic heat pump (THP) is a heat pumping (or refrigeration) device, featuring the advantages of high reliability and low manufacturing costs due to the lack of moving parts, as well as being environmentally-benign. In a THP, acoustic power is used to produce pressure oscillations, while the thermoacoustic conversion occurs in the stack or regenerator of the THP, where the interplay between pressure, velocity and temperature oscillations near the boundary layer generates a time-averaged, non-zero heat flux up the temperature gradient, i.e., thermoacoustic cooling effect [3]. An early experimental demonstration on this effect was performed by Gifford and Longworth [4], who observed heat pumping within a straight tube, in the presence of

pressure oscillations. In a subsequent study, Feldman and Carter [5] discovered that the thermoacoustic conversion could be significantly enhanced by introducing a porous medium (often referred to as a stack or regenerator) into a thermoacoustic system, due to the increased surface area available for conversion. Since then, efficient THPs with up to hectowatt-scale [6] and kilowatt-scale cooling power [7], and with more than 100 K temperature drop [8] have been developed, indicating applications in space expeditions [9], off-shore gas liquefaction [10] and heat recovery [11].

Early THPs were of a standing-wave type, characterized by a straight tube resonator, which forms a standing-wave acoustic field. The thermodynamic cycle in these devices requires imperfect thermal contact between the gas and the solid, resulting in an inherent irreversibility that substantially limits the efficiency. In a typical acoustic-driven, standing-wave THP, the highest coefficient of performance (*COP*) was only 16% of the Carnot cycle [9]. During the last two decades, THPs based on the travelling-wave thermoacoustic conversion, characterized with a looped resonator, have been developed. They are expected to be

* Corresponding author.

E-mail address: ramong@technion.ac.il (G.Z. Ramon).

<https://doi.org/10.1016/j.enconman.2021.115202>

Received 15 August 2021; Received in revised form 29 December 2021; Accepted 30 December 2021

Available online 14 January 2022

0196-8904/© 2022 Elsevier Ltd. All rights reserved.

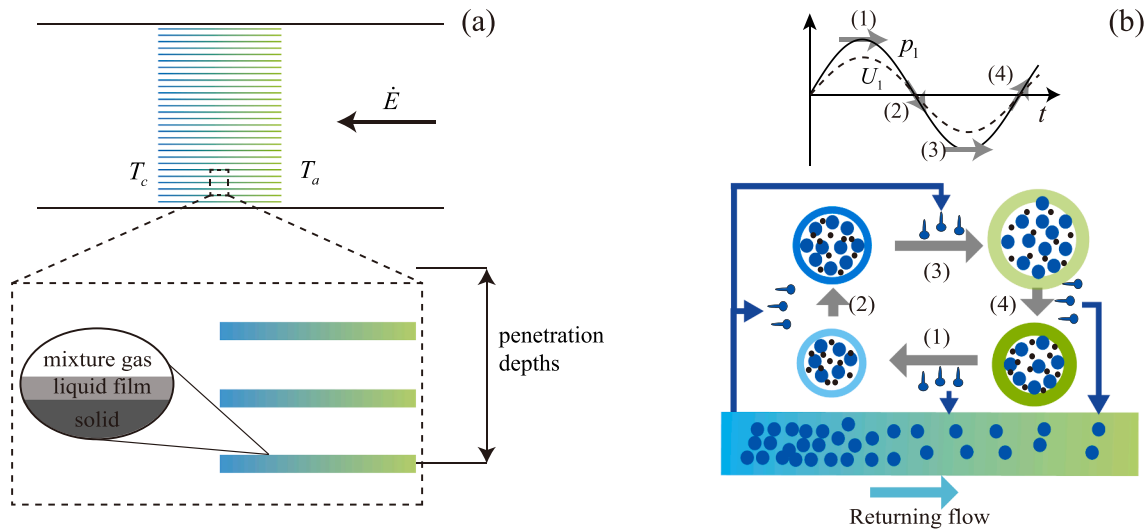


Fig. 1. (a) Geometry of the parallel-plate regenerator. (b) The thermodynamic cycle in a travelling-wave phase-change thermoacoustic heat pump. The four thermodynamic steps: (1) isobaric heat rejection with mass loss, (2) isothermal expansion with mass gain, (3) isobaric heat absorption with mass gain and (4) isothermal compression with mass loss.

more efficient than the standing-wave THPs, because the corresponding thermodynamic cycle can be reversible. For instance, Swift and Wollan [12] reported a travelling-wave THP, whose *COP* relative to Carnot cycle could be as high as 23%. Hofler [13] proposed a heat-driven thermoacoustic heat pump that includes both an engine stage and a heat pump stage—the former consumes heat to generate acoustic power, and the latter consumes acoustic power, provided by the engine stage, to pump heat. This idea has been adopted in many travelling-wave THP systems (see, e.g., [14–18]). In particular, a commercial heat-driven THP developed by SoundEnergy B.V., driven by waste heat in the temperature range of 160–300°C, is able to provide 25–40 kW of cooling power for household use [19]. Systems with similar configuration were also built for natural gas liquefaction, which provided several hundreds watts of cooling power with an overall efficiency of 8% to 10% of the Carnot efficiency [20,21].

Recently, the idea that thermoacoustic conversion can be enhanced by phase change, (which, apparently, was already noted by De la Rive in the 19th century) [22], has regained attention. Rather than using a pure gas phase working fluid, the phase-change thermoacoustic system adopts a binary mixture comprised of an “inert” gas and a “reactive” component that undergoes reciprocating mass exchange with the solid boundary during the oscillation, as the working fluid. In an acoustic field, the partial pressure oscillation of the reactive component induces mass exchange between the gas and the solid wall, via gas–liquid phase change [23]. As a result, the heat flux and volumetric velocity oscillations are amplified, and the thermoacoustic conversion is enhanced accordingly. This enhancement was modelled by Raspét et al. [24,25], and later verified in thermoacoustic engines both theoretically and experimentally [26,27,23,28,29]. Further, the phase-change thermoacoustic conversion can also be used to improve the performance of a THP, as revealed by Slaton et al. [30] through an ideal theoretical analysis on a standing-wave THP. Yang et al. [31] built a phase-change standing-wave THP, observing a twofold increase of the *COP* through the introduction of phase change.

To date, an investigation of phase-change thermoacoustic heat pumping in a travelling-wave acoustic field, which is potentially more efficient than in a standing-wave field, has yet to be performed. Herein, we present a theoretical study on travelling-wave phase-change thermoacoustic heat pumping, using both an ideal model (a short heat pump

in a pure travelling-wave field), and a full numerical analysis of a multi-stage thermoacoustic heat pump with a looped configuration. In the analysis of the short heat pump, we examine the influence of the main factors determining the thermoacoustic heat pumping, in order to shed light on the performance of an ideal phase-change travelling-wave heat pump. In the full system analysis, we perform systematic numerical experiments demonstrating the effect of phase change in a practical system. Our results show the potential of the phase-change travelling-wave thermoacoustic heat pump for clean, efficient and low-cost heat pumping, especially for a small temperature difference.

2. Model formulation

2.1. Theory

The acoustic-to-thermal conversion in a travelling-wave system occurs within the regenerator, which is, in general terms, a porous media. In order to maintain good thermal contact between the solid and the gas, the pore hydraulic radius is required to be much smaller than the local penetration depths [32]. As shown in Fig. 1a, heat will be pumped against the direction of the acoustic power, via a thermodynamic cycle that involves phase change in the travelling-wave acoustic field. The cycle is analogous to a reverse Ericsson cycle, as shown in Fig. 1b. In this 4-step cycle, acoustic power is consumed in order to pump heat against the temperature gradient. Beginning from step (1), the mixture parcel, comprising a reactive component (that undergoes phase change between fluid and gas), and an inert gas, moves toward the lower temperature region isobarically, and rejects heat into the solid. Further, the lowered saturation vapor pressure caused by the temperature drop drives condensation of the reactive component onto the liquid film on the solid surface. In step (2), the parcel expands as the pressure decreases. Some reactive component evaporates from the liquid film into the parcel, carrying latent heat with it. Finally, in steps (3) and (4), the parcel undergoes the reverse processes of steps (1) and (2), whereby the parcel moves back along the direction of wave propagation. Mass, and latent heat, are therefore shuttled along the regenerator, creating and maintaining a temperature difference.

The theoretical description of phase-change thermoacoustic conversion was first developed by Raspét et al. [25] and Slaton et al. [30],

who introduced the effects of phase change and diffusion into Rott's linear thermoacoustic theory. This model was expanded by Weltsch et al. [33] and Offner et al. [23] to describe the thermoacoustic conversion incorporated with mass exchange process between working fluid and solid surface, including condensation/evaporation but also extendable to reversible reactions such as absorption or adsorption. The theory was validated against experiments in some phase-change thermoacoustic systems [26,28,31]. Herein, we use the dimensional form of the equations formulated in Offner et al. [23] to model the phase-change thermoacoustic heat pump.

The governing equations for momentum, continuity, total power and energy transfer are given as

$$\frac{dp_1}{dx} = -\frac{i\omega\rho_m}{F_\nu A_{\text{gas}}} U_1, \quad (1)$$

$$\begin{aligned} \frac{dU_1}{dx} = & -\frac{i\omega A_{\text{gas}}}{\rho_m a^2} \left[\gamma + F_\alpha \left(1 - \gamma \right) + \gamma \frac{C_m}{1 - C_m} \frac{1 - F_D}{\eta_D} \right] p_1 \\ & + \left[\frac{F_\nu - F_\alpha}{(1 - Pr)F_\nu} \beta + \frac{\eta_\nu (1 - F_D) - (1 - F_\nu)}{F_\nu (1 - Sc)} \frac{C_m}{1 - C_m} \frac{l_h}{R_g T_m^2} \right] \frac{dT_m}{dx} U_1, \end{aligned} \quad (2)$$

$$\frac{dT_m}{dx} = \frac{\dot{H}_2 - \frac{1}{2} \Re \left[p_1 \tilde{U}_1 \left(1 - \frac{\tilde{F}_\nu - \tilde{F}_\alpha}{(1 + Pr)F_\nu} \right) \right] - \dot{m} l_h}{\frac{\rho_m c_p |U_1|^2}{2A_{\text{gas}} \omega (1 - Pr) |F_\nu|^2} \Im \left[\frac{\tilde{F}_\nu - \tilde{F}_\alpha}{1 + Pr} - \tilde{F}_\nu \right] - (A_{\text{gas}} k + A_s k_s)}, \quad (3)$$

$$\frac{d\dot{H}_2}{dx} = \dot{q}, \quad (4)$$

where p_1 and U_1 are the amplitudes of the pressure and volumetric velocity, respectively. \dot{H}_2 is the total energy flux, where the subscript "2" indicates a second-order quantity. $T_m, \rho_m, a, c_p, \gamma, \beta, Pr$ and Sc denote the mean temperature, the density, the speed of sound, the heat capacity, the specific heat ratio, the thermal expansion coefficient, the Prandtl number and the Schmidt number of the mixture, respectively, R_g is the universal gas constant, ω is the angular frequency, k and k_s represent the thermal conductivity of the gas and solid, respectively, l_h is the latent heat of the reactive component and A_{gas} and A_s represent the cross-sectional area for gas and solid, respectively. The parameters η_ν and η_D account for generalized sorption kinetics, and reduce to unity in the gas-liquid phase change considered herein [23]. The symbols \Re and \Im denote the real and imaginary parts of a complex number. \dot{q} , the change rate of \dot{H}_2 along the axial direction, is zero in all components except in heat exchangers. \dot{m} is the time-averaged mass flux, which can be calculated by [33]

$$\begin{aligned} \dot{m} = & \frac{1}{1 - C_m} \frac{C_m}{2R_g T_m} \Re \left[p_1 \tilde{U}_1 \frac{F_D - \tilde{F}_\nu}{(1 + Sc)\tilde{F}_\nu} \right] \\ & - \frac{1}{1 - C_m} \frac{|U_1|^2}{2A_{\text{gas}} \omega |F_\nu|^2} \frac{p_m C_m l_h}{R_g^2 T_m^3} \frac{1}{1 - Sc^2} \Im \left[\tilde{F}_\nu \left(1 + Sc \right) + \frac{\eta_\nu}{\eta_D} \left(F_D - \tilde{F}_\nu \right) \right] \frac{dT_m}{dx} \\ & - \frac{p_m A_{\text{gas}} D}{1 - C_m} \frac{C_m l_h}{R_g^2 T_m^3} \frac{dT_m}{dx}. \end{aligned} \quad (5)$$

Note that \dot{m} represents the mass flux of the reactive component in the gas phase, which equals (but with an opposing direction) the mass flux of

the liquid required to reach a balance within the regenerator (see the returning flow in Fig. 1(b)) [30]. The mean concentration of the reactive component is determined by the Clausius–Clapeyron relation

$$C_m = \exp \left[-\frac{l_h}{R_g} \left(\frac{1}{T_m} - \frac{1}{T_b} \right) \right], \quad (6)$$

where T_b is the boiling temperature of the reactive component. The functions F_n ($n = \alpha, \nu$ or D) for a parallel-plate regenerator used in this work can be expressed as [12]

$$F_n = 1 - \frac{\tanh \left[(1 + i) \tau_n / \sqrt{2} \right]}{(1 + i) \tau_n / \sqrt{2}} \quad (7)$$

Additionally, by rearranging Eq. (2), a thermoacoustic sink term can be derived: [28]

$$g = \left[\frac{F_\nu - F_\alpha}{(1 - Pr)F_\nu} \frac{1}{T_m} + \frac{\eta_\nu (1 - F_D) + F_\nu - 1}{F_\nu (1 - Sc)} \frac{C_m}{1 - C_m} \frac{l_h}{R_g T_m^2} \right] \nabla T_m. \quad (8)$$

This term directly contributes to the thermoacoustic conversion [12], and will be used in the forthcoming discussion of the system.

2.2. The short heat pump approximation

The acoustic field is one of the most important factors controlling thermoacoustic conversion, since it determines the phasing between reciprocating motion and compression/expansion, much like a piston. In a travelling-wave thermoacoustic system, the acoustic wave is actually not a pure travelling wave, but is dominated by the travelling-wave component (while also containing a standing-wave component). The relative travelling-to-standing wave component is reflected by the phase difference between p_1 and U_1 . This phase difference, and the acoustic impedance (defined as $z = p_1 A_{\text{gas}} / U_1$), are very sensitive to the change of geometry and working conditions of the system, and are consequently different in various systems [20,21,34]. In order to reduce the dependence on these and focus on the effect of phase change, we formulate an ideal model of a phase-change travelling-wave heat pump (much like the 'short engine' approximation in Swift [35]), which is a regenerator with a length Δx , short compared with the wavelength, such that the values of p_1, U_1 and T_m in the heat pump can be considered independent of x . The acoustic field is assumed to be a pure travelling wave, i.e., the phase difference between p_1 and U_1 is zero.

The acoustic power consumed in the 'short' heat pump is given by [12]

$$\Delta \dot{E} = -\frac{\Delta x}{2} \Re \left\{ p_1 \frac{d\tilde{U}_1}{dx} + \frac{dp_1}{dx} \tilde{U}_1 \right\} \quad (9)$$

Plugging Eqs. (1) and (2) into Eq. (9), we have

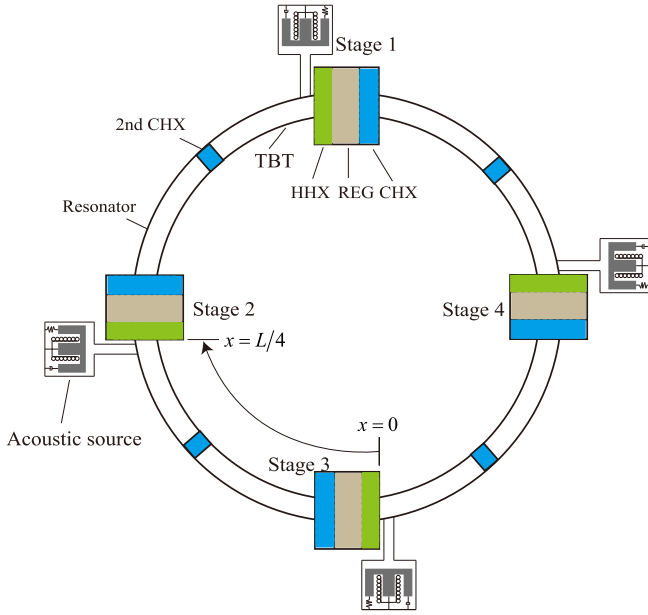


Fig. 2. Schematic of the phase-change travelling-wave thermoacoustic heat pump. It consists of four identical stages, each containing a hot heat exchanger (HHX), a regenerator (REG), a cold heat exchanger (CHX), a secondary cold heat exchanger (2nd CHX), a thermal buffer tube (TBT), and an acoustic source. L is the total loop length.

Table 1

Specifications of the phase-change travelling-wave thermoacoustic heat pump. HHX-hot heat exchanger. REG-regenerator. CHX-cold heat exchanger. 2nd CHX-secondary cold heat exchanger. TBT-thermal buffer tube. ζ -porosity, defined as $\zeta \equiv \frac{A_{gas}}{(A_{gas} + A_s)}$. r_h -hydraulic radius. h -heat transfer coefficient.

| Items | Diameter (mm) | Length (mm) | Details |
|-----------|---------------|-------------|---|
| HHX | 132 | 10 | Parallel-plate heat exchanger, ζ is 0.76, r_h is 0.4 mm. h is assumed to be infinite. |
| REG | 132 | 12 | Parallel-plate regenerator, ζ is 0.8, r_h varies to satisfy specific τ_v |
| CHX | 132 | 20 | Parallel-plate heat exchanger, ζ is 0.76, r_h is 0.5 mm. h is assumed to be infinite. |
| TBT | 26 | 400 | - |
| 2nd CHX | 26 | 20 | Parallel-plate heat exchanger, ζ is 0.8. r_h is 0.5 mm. h is assumed to be infinite. |
| Resonator | 26 | 440 | - |

Thus, the COP of the device, within the limits of this ideal model, can be expressed as

$$COP = \frac{Q_c}{\Delta \dot{E}}, \quad (12)$$

and the corresponding COP under the Carnot cycle is

$$COP_{carnot} = \frac{T_m}{L} \frac{\Delta x}{\Delta T_m}. \quad (13)$$

The COP relative to Carnot is defined as

$$COP_R = \frac{COP}{COP_{carnot}} \quad (14)$$

By substituting Eqs. (10) and (13) into Eq. (14), neglecting the axial heat conduction and diffusion (which becomes increasingly inaccurate, generally speaking, as ∇T_m increases), we find that COP_R depends on 6 factors, namely,

$$COP_R = \mathcal{F} \left(p_m, \frac{\nabla T_m}{\omega}, |z|, \tau_v, C_m, \text{mixture properties} \right), \quad (15)$$

where $\tau_v = r_h \sqrt{\omega/\nu}$ is the Womersley number, ∇T_m is the temperature gradient and $z = p_1 A_{gas}/U_1$ is the acoustic impedance. The detailed expression of Eq. (15) can be found in the appendix. Further, this simplified model shows that COP_R weakly depends on p_m (see the appendix). Hence, the number of main factors determining COP_R is reduced to 5: $\tau_v, \frac{\nabla T_m}{\omega}, |z|, C_m$ and the mixture properties.

Additionally, as can be seen, for an ideal travelling-wave refrigerator, if we neglect viscous losses, such that $F_v = 1, F_D = F_\alpha = 0, Sc = Pr = 0$, we get $COP_R = 1$, which means its efficiency can theoretically reach that of the Carnot cycle.

2.3. Numerical simulation of a multi-stage heat pump system

While providing simple insight, the short heat pump model is based on several assumptions, which may be far from a real travelling-wave heat pump system. In this section, we develop a model of a far more realistic, phase-change travelling-wave thermoacoustic heat pump (PTTHP), so as to probe its projected performance. As shown in Fig. 2, the PTTHP consists of four identical stages. Each stage includes a regenerator, two heat exchangers, a secondary ambient heat exchanger, a thermal buffer, a resonator, and an acoustic source (for example, a linear alternator). The detailed dimensions of each component are listed in Table 1. This looped configuration has already been proven to be an established design, able to achieve an acoustic field dominated by the travelling-wave component [11]. When under operation, the acoustic power from the acoustic source is delivered to the adjacent thermoacoustic stage, where the acoustic power is consumed to pump heat from

$$\Delta \dot{E} = -\frac{\Delta x}{2} \Re \left\{ \frac{A_{gas} \gamma \omega^2}{i \omega \rho_m a^2} |p_1|^2 \left[\frac{\gamma - 1}{\gamma} \tilde{F}_\alpha + \frac{C_m}{1 - C_m} \tilde{F}_D \right] - \frac{1}{T_m} \frac{dT_m}{dz} \left[\frac{\tilde{F}_\alpha - \tilde{F}_v}{(1 - Pr) \tilde{F}_v} + \frac{l_h}{R_g T_m} \frac{C_m}{1 - C_m} \frac{\tilde{F}_D - \tilde{F}_v}{(1 - Sc) \tilde{F}_v} \right] p_1 \tilde{U}_1 + \frac{i \omega \rho_m}{A_{gas}} \frac{|U_1|^2}{\tilde{F}_v} \right\}. \quad (10)$$

The cooling power of the short heat pump can be calculated by [32]

the cold end to the ambient end. A binary mixture, including one inert gas (helium) and one reactive component (ammonia) is used as the

$$Q_c = \dot{E}_c - \dot{H}_2 = -\frac{dT_m}{dx} \left\{ \frac{\rho_m c_p |U_1|^2}{2 A_{gas} \omega (1 - Pr) |F_v|^2} \Im \left[\frac{\tilde{F}_v - F_\alpha}{1 + Pr} - \tilde{F}_v \right] - (A_{gas} k + A_s k_s) - \dot{m} l_h + \frac{1}{2} \Re \left[p_1 \tilde{U}_1 \frac{\tilde{F}_v - F_\alpha}{(1 + Pr) \tilde{F}_v} \right] \right\}. \quad (11)$$

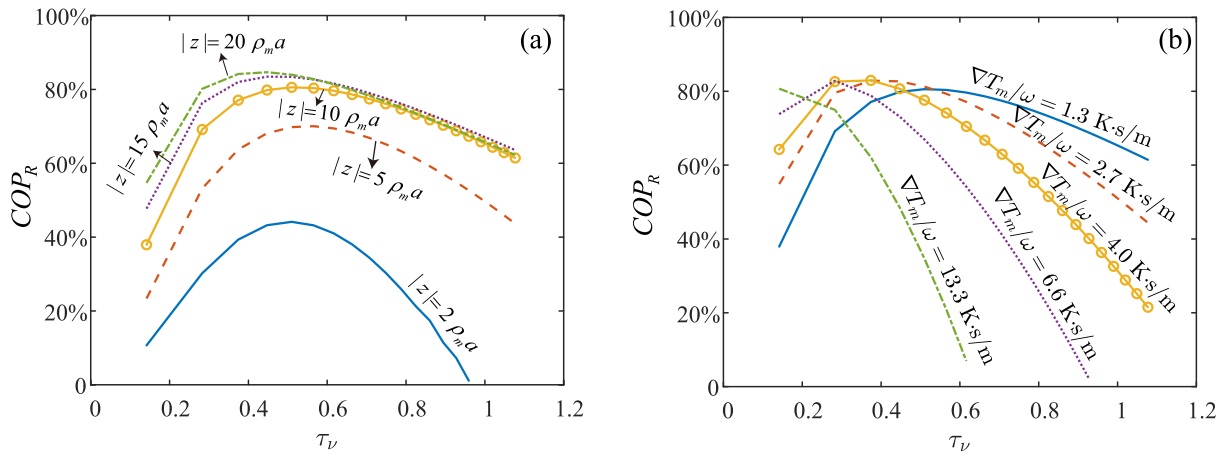


Fig. 3. The relation between COP_R and τ_v of the short heat pump in a pure travelling-wave field, at different values of $|z|$ in (a) and $\nabla T_m/\omega$ in (b). The working mixture is helium and water, $p_m = 10$ bar, $C_m = 0.4$.

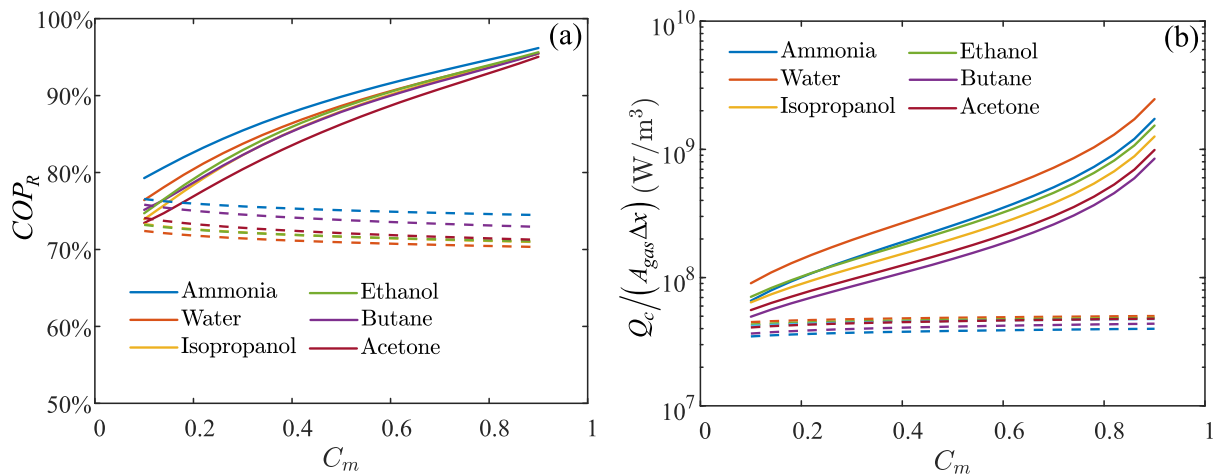


Fig. 4. Performance of the short heat pump in a pure travelling-wave field, at varying values of C_m , the concentration of the reactive component. The solid and dashed lines represent wet and dry cases, respectively. (a) COP_R - coefficient of performance relative to Carnot. (b) Specific cooling power, $Q_c/(A_{gas}\Delta x)$. 6 materials are used as the reactive component respectively, while the inert gas is fixed as helium. The mean pressure is $p_m = 10$ bar and the acoustic impedance is $|z| = 30 \rho_m a$. The value of τ_v , or r_h , has been optimized at every point to reach the highest COP_R , $\frac{\nabla T_m}{\omega} = 1.33K\cdot s/m$. For the dry cases, the horizontal axis C_m denotes the corresponding T_m according to Eq. (6).

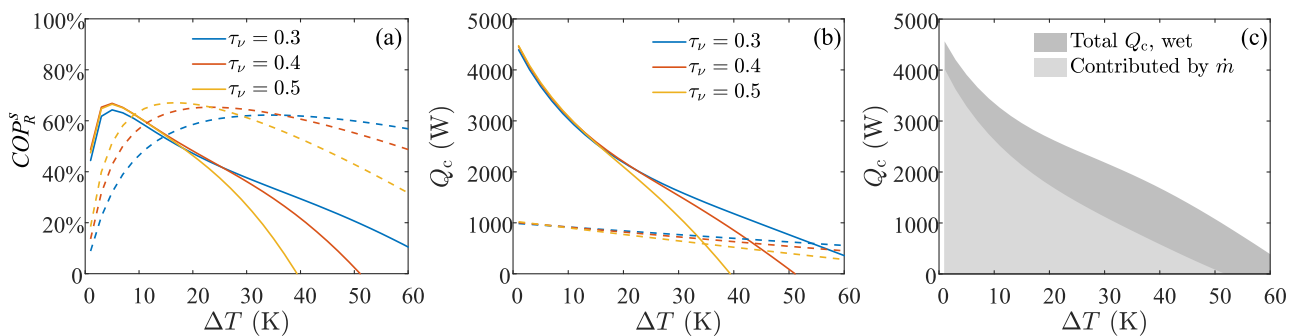


Fig. 5. A comparison between the performance of the system under wet and dry modes of operation. (a) The dependence of COP_R^s on the temperature difference, with different Womersley number τ_v ($\tau_v = r_h\sqrt{\omega/\nu}$). (b) The dependence of cooling power on temperature difference. (c) The contribution of the mass flux to the total cooling power. In (a) and (b), the solid and dashed lines represent the wet and dry cases, respectively. The working fluid is helium in the dry mode, with a helium/ammonia mixture in the wet mode. $C_{m,a} = 0.5$ ($T_a = 276$ K). $p_m = 10$ bar. $|p_1|$ at the hot end of the regenerator is set to be 3% of the mean pressure.

working fluid.

In the model of this system, several assumptions were made: First, the temperature gradient is assumed zero in the resonator and heat ex-

changers. Second, the total energy flow \dot{H}_2 is assumed to be constant along the resonator, thermal buffer tube and the regenerator, which represents perfect thermal insulation in these components. Finally, the

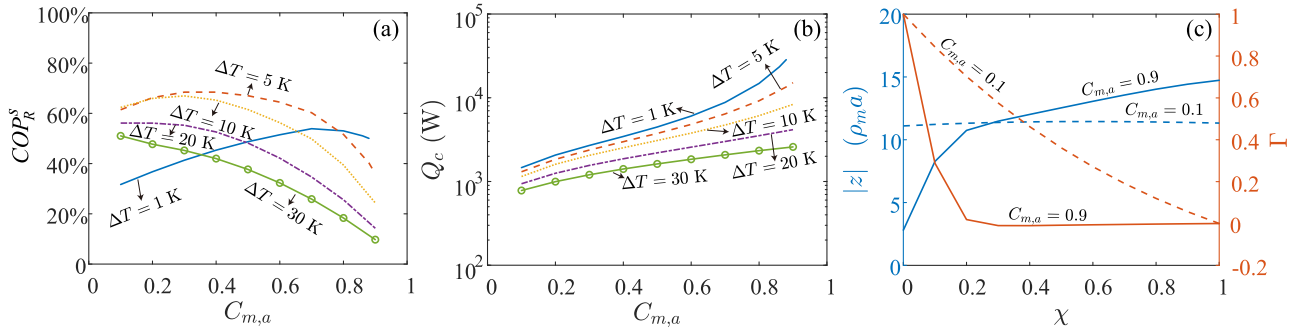


Fig. 6. The performance of the PTHP under different concentration of the reactive component, $C_{m,a}$, at the hot end. (a) The dependence of COP_R^s on $C_{m,a}$, at different temperature differences. (b) The dependence of cooling power, Q_c , on $C_{m,a}$, at different temperature differences. (c) The distributions of acoustic impedance and temperature (normalised) in the regenerator. $\chi = \Delta x/l_r$ is the normalised location of the regenerator, where Δx is the distance to the cold side, and l_r is the length of the regenerator. $\Gamma = (T - T_c)/\Delta T$ is the normalized temperature. $p_m = 10$ bar. $|p_1|$ at the hot end of the regenerator is set to be 3% of the mean pressure.

heat transfer coefficient between the gas mixture and the solid of the heat exchangers is infinite. Given the symmetry of the four identical stages, only one stage was calculated by adopting periodical boundary conditions, i.e.,

$$|p_1|_{x=0} = |p_1|_{x=L/4}, \quad (16a)$$

$$|U_1|_{x=0} = |U_1|_{x=L/4}, \quad (16b)$$

$$ph(p_1)_{x=0} = ph(p_1)_{x=L/4} + 90^\circ, \quad (16c)$$

$$ph(U_1)_{x=0} = ph(U_1)_{x=L/4} + 90^\circ, \quad (16d)$$

$$T_{m,x=0} = T_{m,x=L/4}. \quad (16e)$$

The symbol ph denotes the phase angle of a complex number. By integrating Eqs. (1)–(4) with a fourth-order Runge–Kutta routine, and targeting the boundary conditions, the distributions of p_1 , U_1 and T_m and \dot{H}_2 along the system can be obtained. The acoustic power is then calculated by $\dot{E}_2 = \frac{1}{2} \Re [p_1 \tilde{U}_1]$. The cooling power Q_c is taken as the difference of \dot{H}_2 between the two ends of the cold heat exchanger.

We then define the coefficient of performance of the system

$$COP^s = \frac{Q_c}{\Delta E_r} \quad (17)$$

where ΔE_r is the acoustic power difference between the two ends of the regenerator.

The relative Carnot coefficient of performance is defined as

$$COP_R^s = \frac{COP^s \Delta T}{T_c} \quad (18)$$

where $\Delta T = T_h - T_c$, and T_h and T_c are the temperatures at the hot and cold end of the regenerator, respectively.

3. Results and discussion

3.1. Short heat pump

We begin by examining the main parameters affecting the process, using the simplified model, which enables straightforward insight. In what follows, we discuss how these factors affect COP_R , and the required conditions for achieving high performance.

In Fig. 3, we present the dependence of COP_R on the Womersley

number, τ_ν , with different values of acoustic impedance $|z|$ in (a), and with different $\frac{\sqrt{T_m}}{\omega}$ shown in (b). The parameter $\tau_\nu = r_h \sqrt{\omega/\nu}$ represents the ratio of the viscous time scale (r_h^2/ν) to the oscillation time scale ($1/\omega$). In order to achieve an efficient thermoacoustic conversion in the travelling-wave field, $\tau_\nu < 1$ is required, otherwise the process shown in Fig. 2b cannot be completed [36]. However, if τ_ν is too small, viscous dissipation becomes dominant, leading to significant losses. For this reason, all curves in Fig. 3a demonstrate a peak around τ_ν of $\sim 0.4 - 0.6$. Furthermore, it can be seen that a high acoustic impedance ($\sim 10 - 30 \rho_m a$, recommended by Gardner and Swift [37]) helps improve COP_R , since it reduces the relative impact of viscous losses. In Fig. 3b, it can be seen that the highest COP_R are $\sim 80\%$, for all curves, with different $\frac{\sqrt{T_m}}{\omega}$, but the corresponding optimal τ_ν decreases as $\frac{\sqrt{T_m}}{\omega}$ increases. Moreover, the value of COP_R becomes more sensitive to τ_ν as $\frac{\sqrt{T_m}}{\omega}$ increases, which may pose a challenge for a PTHP working with large temperature differentials, because slight deviations of τ_ν from the optimal value can severely impact its performance.

In a pure standing-wave field, the enhancement of phase change on COP_R can be readily shown through a simple equation [30]. However, in a travelling-wave heat pump, the enhancement is more obscure because there is no such simple expression. In order to clearly show the effects of phase change, in Fig. 4, we compare the values of COP_R of the short heat pump between wet (with phase change) and dry (without phase change) modes, in a pure travelling-wave field at various values of C_m , with 6 different reactive components. Note that in the dry cases, $C_m \equiv 0$, thus the horizontal axis C_m denotes the corresponding T_m , according to Eq. (6).

The values of COP_R in Fig. 4a can be considered as the upper limit achievable by the heat pump at the specific C_m and $\frac{\sqrt{T_m}}{\omega}$, because τ_ν has been optimised for highest COP_R at every point (the corresponding hydraulic radius r_h is shown in the appendix), and the sensitivity to $|z|$ is small because it is already fixed at a rather large value (see Fig. 3a). It can be seen that the values of COP_R in both dry and wet modes can exceed 70%, owing to the theoretically reversible thermodynamic cycle of the travelling-wave thermoacoustic conversion. However, COP_R in the wet mode becomes increasingly higher than that in the dry mode as C_m increases, verifying the enhancement, due to phase change, of the travelling-wave thermoacoustic conversion. The main reason behind this is that the additional pumped heat introduced by phase change, mainly manifested in the amplified sink term g , far exceeds the accompanied losses (such as the viscous dissipation), which are only weakly affected by the introduction of phase change.

From Fig. 4b, we see that the specific cooling power $\frac{Q_c}{(\rho_m a \Delta x)}$ in the wet

mode is much higher than that in the dry mode. In particular, it can be one order of magnitude higher when C_m is above 0.6 when ammonia and water are used. The increased cooling power in the wet mode is mainly contributed by the time-averaged mass flux due to phase change, which translates into a heat flux $\dot{m}l_h$. Therefore, the values of $\frac{Q_c}{(A_{\text{gen}}\Delta T)}$ for different reactive components under a specific C_m are mainly determined by the latent heat l_h of the reactive component, and the specific mass flux $\frac{\dot{m}}{(A_{\text{gen}}\Delta T)}$. For instance, the value of $\frac{Q_c}{(A_{\text{gen}}\Delta T)}$ is greatest for water, corresponding with its latent heat being the highest.

To adopt a high C_m is an effective strategy to increase both the COP_R and the cooling power of the heat pump. However, it poses significant engineering challenges, because the mass flux \dot{m} is very high under large C_m (see the appendix), therefore requiring a large amount of liquid to be transferred quickly through the narrow channels of the regenerator without blocking them, enabling the evaporated liquid to be replenished in time at all points in the system. Moreover, the optimal τ_v decreases as C_m increases, resulting in a very small optimal pore size of the regenerator (see the appendix), which may further increase the challenge of proper regenerator design.

3.2. System analysis

Next, we turn to examine the performance of a full PTTHP, in a looped configuration as shown in Fig. 2. In Fig. 5, we show a comparison between the performances of the wet and dry modes of the PTTHP, both at a mean pressure of 10 bar. The pressure amplitude $|p_1|$ at the hot end of the regenerator is set to be 3% of the mean pressure. As can be seen, both modes of operation can reach a $COP_R^s > 60\%$, but with different ranges of ΔT . The COP_R^s of the wet mode peaks at a much smaller ΔT than the dry mode, and decreases rapidly as ΔT increases, eventually leading to a COP_R^s lower than that of the dry mode at a large ΔT . This is mainly ascribed to two reasons. First, in the wet mode, the acoustic impedance $|z|$ near the hot end of the regenerator decreases significantly when ΔT is increased. For example, with $\tau_v = 0.4$, $|z| > 10\rho_m a$ in the entire regenerator when $\Delta T < 10$ K, while $|z|$ near the hot end drops to $6\rho_m a$ when $\Delta T = 40$ K, which increases the viscous loss, and thus decreases COP_R^s . Second, COP_R^s becomes increasingly sensitive to τ_v as ∇T_m (or ΔT) increases, as revealed in Fig. 3b. The inevitable deviation of τ_v from its optimal value causes further reduction of COP_R^s under a large ΔT . A straightforward idea to improve the performance is to reduce ∇T_m by increasing the length of the regenerator, which works, however, with limited effect. When the length is increased, the distribution of the temperature along the regenerator will become increasingly non-linear, which means ∇T_m near the hot end will be significantly larger than that near the cold end. This will decrease $|z|$ near the hot end, offsetting the advantages from increasing the length.

In the phase-change heat pump, there exists a time-averaged mass flux \dot{m} of the reactive component along the regenerator. This mass flux carries a considerable amount of heat (the latent heat of phase change) against the temperature drop, leading to a much higher cooling power Q_c in the wet mode, compared with the corresponding dry case, as shown in Fig. 5b. An example showing the contribution of the mass flux is presented in Fig. 5c. We see that most of the pumped heat is contributed by the mass flux, \dot{m} at a small ΔT , and the contribution of \dot{m} decreases as ΔT is increased. For example, when $\Delta T = 1$ K, the cooling power contributed by \dot{m} accounts for 88% of the total. However, the value of \dot{m} decreases gradually as ΔT increases, finally reaching zero at a ΔT of 51 K. If ΔT is increased further, \dot{m} will reverse its direction, therefore acting against the heat pumping, leading to a Q_c lower than that in the dry mode. A similar effect has been observed in a phase-

change standing-wave heat pump [30,31].

In Fig. 6, we show the performance of the PTTHP under different concentrations of the reactive component, $C_{m,a}$, at the hot end of the regenerator, at various values of ΔT . In accordance with the results of the ideal model shown in Fig. 4, the cooling power Q_c rises significantly as more reactive component is involved (with the increase of $C_{m,a}$). However, in contrast to the ideal model, COP_R^s of the PTTHP begins to fall when $C_{m,a}$ exceeds some critical value, which means that a high concentration doesn't necessarily bring about a high COP_R^s . Further, the larger ΔT is, the smaller the critical C_m , at which COP_R^s peaks, becomes. For example, the critical value is $C_m = 0.7$ when $\Delta T = 1$ K, while it is smaller than 0.1 when $\Delta T = 30$ K. This indicates that when ΔT is large, the strong contribution of phase change under a large C_m may result in deteriorated performance of the presented system. The main reason behind is that the acoustic impedance, $|z|$, near the hot end, where most of the temperature drop occurs (see Fig. 6c), is far smaller than the suggested value in Gardner and Swift [37], when C_m is high. As shown in Fig. 6c, when $C_m = 0.1$, $|z| \sim 11\rho_m a$ in the whole regenerator including the hot end, while when $C_m = 0.9$, $|z| \sim 3\rho_m a$ at the hot end, leading to significant viscous losses.

The disadvantageous distribution of $|z|$ is caused by the non-constant heat pumping ability of the regenerator along the axial direction of the regenerator with high C_m , which can be characterised by the thermoacoustic sink term g (see Eq. (8)). In the regenerator, the value of C_m at the hot end is the highest (see Eq. (6)), as is ∇T_m (reflected by the curve of the dimensionless temperature Γ in Fig. 6c), resulting in the sink term g being correspondingly larger near the hot end, compared with the rest of the regenerator. As a result, the volumetric velocity U_1 near the hot end decays much faster along the direction of propagation, compared with the rest of the regenerator, to satisfy the "consumption" of the strong sink term. This means that U_1 at the hot end is much larger than anywhere else, leading to a very low $|z|$ near the hot end of the regenerator. In contrast, g is almost constant throughout the regenerator of the dry system, such that U_1 and p_1 decrease with similar rates along the regenerator, leading to a near-constant distribution of $|z|$.

Increasing the acoustic impedance, $|z|$, in the regenerator had been a major problem encountered during early stages of travelling-wave thermoacoustic system development [38], and it appears to have become a challenge once again, for the phase-change systems. A commonly used technique in classical travelling-wave thermoacoustic systems is to locally enlarge the cross section of the regenerator [11]. Unfortunately, further increasing the cross sectional area of the regenerator in this PTTHP, or only the hot part of the regenerator (e.g., using an exponentially-varying cross section) shows very limited improvement when $C_{m,a}$ is high, because g near the hot end is also increased, offsetting the effort to increase $|z|$. Hence, to fully utilize the advantage of phase change in thermoacoustic heat pumping, the current design of PTTHP is suitable for applications with small temperature difference, which may include ice production, distillation, industrial heating, etc [39].

4. Conclusions

In this work, we have investigated the performance of a phase-change thermoacoustic heat pump, using both an idealized, short heat pump model with a pure travelling-wave field, as well as a full, looped-tube thermoacoustic heat pump system. In the analysis of the short heat pump, we identified and investigated the influence of the main parameters - the acoustic impedance, the ratio of temperature gradient over the angular frequency, Womersley number, the concentration of the reactive component, and the reactive species, on the thermoacoustic

heat pumping. These results shed light on the performance of an ideal travelling-wave phase-change heat pump. Meanwhile, the analysis of the full system provides a more practical view of such a device.

Importantly, the results from the ideal model (the short heat pump) demonstrate the full potential of a phase-change thermoacoustic heat pump. We find that the cooling power can be increased by up to one order of magnitude, compared with the dry mode, through the introduction of phase change. The COP_R , representing the efficiency of the short heat pump relative to the Carnot efficiency, can also be improved but at a small increment, since COP_R in the dry mode can already exceed 70% so there is not much room for further improvement. In order to attain the potential enhancement of phase change, stringent requirements on the acoustic impedance and the Womersley number must be satisfied, especially under a large ratio of the temperature gradient over the angular frequency, otherwise the performance may deteriorate significantly.

Further, in the analysis of the full system operating with a high concentration of the reactive component, an increase of COP_R^s , representing the efficiency of the system relative to the Carnot efficiency, is only achieved by introducing phase change under small temperature differences (below 10 K). As the temperature difference is increased, COP_R^s decreases, eventually becoming lower than that achieved without phase change. This effect becomes increasingly significant as the concentration of the reactive component increases, mainly because the acoustic impedance near the ambient end of the regenerator drops significantly at high concentrations and a large temperature difference, leading to severe viscous losses. Increased cooling power, while also inversely dependent on the temperature difference, can be achieved by phase change over a wide range of temperature differences (beyond 50

K).

The proposed phase-change looped thermoacoustic system may be used in applications where small temperature differences are required, including ice making, distillation, industrial heating, etc. Future designs for efficient large temperature difference heat pump are possible, using cascading stages, with each stage pumping heat from the cold end of the previous stage.

CRedit authorship contribution statement

Rui Yang: Conceptualization, Methodology, Software, Data curation, Investigation, Writing - original draft. **Nathan Blanc:** Methodology, Software, Writing - original draft. **Guy Z. Ramon:** Conceptualization, Supervision, Writing - review & editing, Project administration, Funding acquisition.

Declaration of Competing Interest

The authors declare that they have no known competing financial interests or personal relationships that could have appeared to influence the work reported in this paper.

Acknowledgments

The research was supported by grant 219-11-127 from the Israel Ministry of Energy and Water. R.Y. was supported, in part, by a fellowship from the Israel Council for Higher Education. N.B. acknowledges the support provided by the Grand Technion Energy Program (GTEP).

Appendix A

A.1. Derivation of Eq. (15)

Eq. (15) can be re-expressed as

$$COP_R = \frac{2}{T_m} \frac{-\frac{\nabla T_m}{\omega} \left\{ \frac{\rho_m c_p}{2(1-Pr)|F_v|^2} \Im \left[\frac{(\tilde{F}_v - F_a)}{(1+Pr)} - \tilde{F}_v \right] \right\} - \frac{\dot{m}_h}{|v_1|^2 A_{gas}} + \frac{1}{2} \Re \left[\frac{v_1 v_1^*}{|v_1|^2} \left(\frac{\tilde{F}_v - F_a}{(1+Pr)F_v} \right) \right]}{\Re \left\{ \frac{1}{\omega} \frac{\gamma}{i\alpha^2 \rho_m} |z|^2 \left[\frac{\gamma-1}{\gamma} \tilde{F}_a + \frac{C_m}{1-C_m} \tilde{F}_D \right] - \frac{1}{T_m} \left\{ \frac{\tilde{F}_a - \tilde{F}_v}{(1-Pr)F_v} + \frac{l_h}{R_g T_m} \frac{C_m}{1-C_m} \frac{\tilde{F}_D - \tilde{F}_v}{(1-Sc)F_v} \right\} |z| + \frac{i p_m}{\omega} \frac{1}{F_v} \right\}} \quad (A.1)$$

If we ignore the heat conduction in axial direction, and neglecting the diffusive loss (might be inaccuracy with large ∇T_m), the term $\frac{\dot{m}_h}{|v_1|^2 A_{gas}}$ in Eq. (A.1) can be expressed as

$$\frac{\dot{m}_h}{|v_1|^2 A_{gas}} \approx \frac{l_h}{1-C_m} \frac{C_m}{2R_g T_m} |z| \Re \left[\frac{F_D - \tilde{F}_v}{(1+Sc)\tilde{F}_v} \right] - \frac{C_m}{1-C_m} \frac{1}{2|F_v|^2} \frac{p_m l_h^2}{R_g^2 T_m^3} \frac{1}{1-Sc^2} \Im \left[\tilde{F}_v (1+Sc) + (F_D - \tilde{F}_v) \right] \frac{\nabla T_m}{\omega} \quad (A.2)$$

Additionally, F_n is a function of τ_v , and T_m can be determined by C_m (Eq. 6). Thus, Eq. A.1 shows that COP_R can be determined by 6 factors, as shown in Eq. (15).

A.2. COP_R weakly depends on p_m

As shown in Fig. A.1, the value of COP_R weakly depends on p_m , especially when τ_v is the optimal value. A.2.

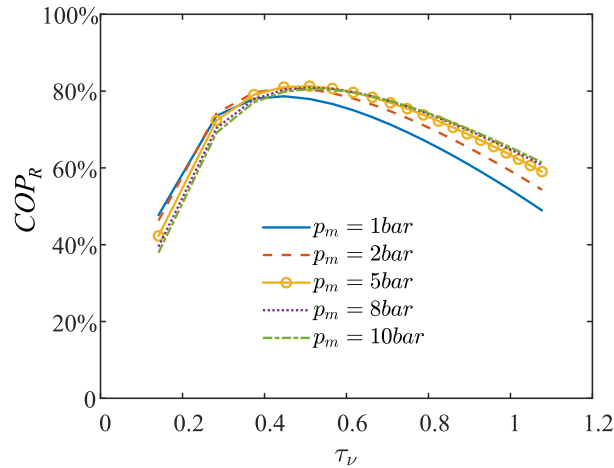


Fig. A.1. Influence of mean pressure. $p_m = 10$ bar, $\phi = 0^\circ$, $C_m = 0.4$.

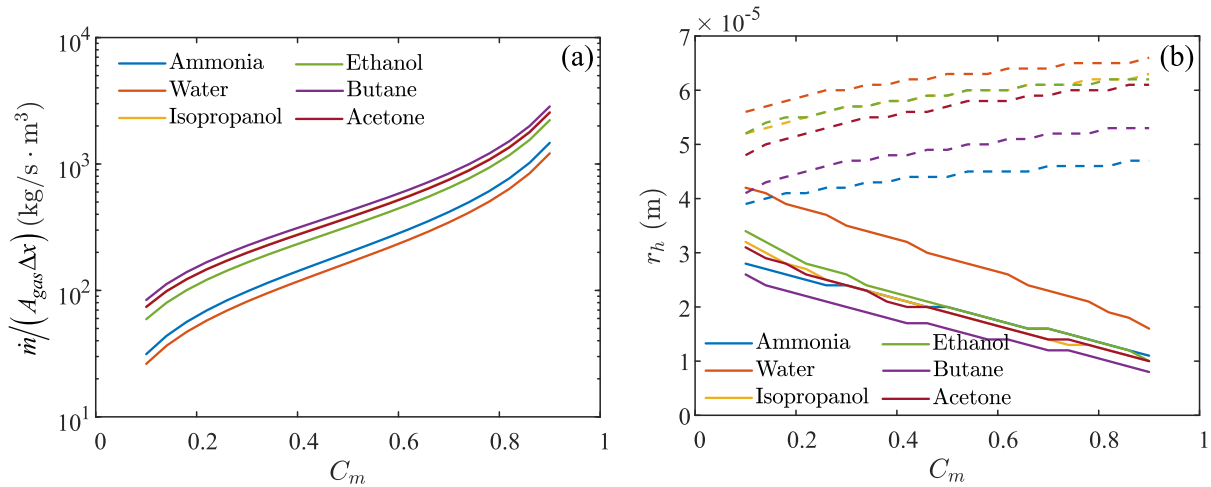


Fig. A.2. Supplementary data of the results shown in Fig. 4. (a) Specific mass flux $\dot{m}/(A_{\text{gas}}\Delta x)$ vs. C_m . (b) Hydraulic radius r_h vs. C_m . 6 materials are used as the reactive component relatively. The inert gas is helium. $p_m = 10$ bar. $|z| = 30 \rho_m \alpha$. The value of τ_ν , or r_h , has been optimized at every point to reach the highest COP_R . $\frac{\nabla T_m}{\omega} = 1.33\text{K}\cdot\text{s}/\text{m}$. The solid and dashed lines represent wet and dry cases, respectively. For the dry cases, the horizontal axis C_m just denotes the corresponding T_m according to Eq. (6).

References

- [1] Davis LW, Gertler PJ. Contribution of air conditioning adoption to future energy use under global warming. *Proceedings of the National Academy of Sciences* 2015; 112(19):5962–7.
- [2] Razmi A, Soltani M, Torabi M. Investigation of an efficient and environmentally-friendly CCHP system based on CAES, ORC and compression-absorption refrigeration cycle: Energy and exergy analysis. *Energy Conversion and Management* 2019;195:1199–211.
- [3] Chen G, Tang L, Mace B, Yu Z. Multi-physics coupling in thermoacoustic devices: A review. *Renewable and Sustainable Energy Reviews* 2021;146:111170.
- [4] W.E. Gifford, R. Longworth, Surface heat pumping, in: *Advances in Cryogenic Engineering*, Springer, 171–179, 1966.
- [5] K.T. Feldman, R. Carter, A study of heat driven pressure oscillations in a gas.
- [6] Ramadan IA, Bailliet H, Poignand G, Gardner D. Design, manufacturing and testing of a compact thermoacoustic refrigerator. *Applied Thermal Engineering* 2021;189: 116705.
- [7] Wang H, Zhang L, Hu J, Yu G, Wu Z, Dai W, Luo E. Study on a novel looped heat-driven thermoacoustic refrigerator with direct-coupling configuration for room temperature cooling. *International Journal of Refrigeration* 2021;123:180–8.
- [8] Hofler TJ, Wheatley JC, Swift GW, Migliori A. Acoustic cooling engine. *The Journal of the Acoustical Society of America* 1988;84(1):460.
- [9] Garrett SL, Adef J, Hofler TJ. Thermoacoustic refrigerator for space applications. *Journal of thermophysics and heat transfer* 1993;7(4):595–9.
- [10] G.W. Swift, Thermoacoustic natural gas liquefier, Tech. Rep., USDOE Morgantown Energy Technology Center, WV (United States), Los Alamos National Lab. (LANL), 1995.
- [11] K. De Blok, Multi-stage traveling wave thermoacoustics in practice, in: 19th Int. Congress Sound Vibration, Vilnius, Citeseer, 2012.
- [12] Swift G, Wollan J. Thermoacoustics for liquefaction of natural gas. *GasTIPS* 2002;8 (4):21–6.
- [13] T.J. Hoffer, High efficiency heat driven acoustic cooling engine with no moving parts, United States Patent, Patent (5,901,556).
- [14] Luo E, Dai W, Zhang Y, Ling H. Thermoacoustically driven refrigerator with double thermoacoustic-Stirling cycles. *Applied Physics Letters* 2006;88(7):074102.
- [15] Yu B, Luo E, Li S, Dai W, Wu Z. Experimental study of a thermoacoustically-driven traveling wave thermoacoustic refrigerator. *Cryogenics* 2011;51(1):49–54.
- [16] Kang H, Zhou G, Li Q. Heat driven thermoacoustic cooler based on traveling-standing wave. *Energy Conversion and Management* 2010;51(11): 2103–8.
- [17] Yazaki T, Biwa T, Tominaga A. A pistonless Stirling cooler. *Applied Physics Letters* 2002;80(1):157–9.
- [18] Chi J, Xu J, Zhang L, Wu Z, Hu J, Luo E. Study of a gas-liquid-coupled heat-driven room-temperature thermoacoustic refrigerator with different working gases. *Energy Conversion and Management* 2021;246:114657.
- [19] SoundEnergy, THEAC-25 THERMOACOUSTIC ENERGY CONVERTER, [EB/OL], <https://www.soundenergy.nl/our-technology> Accessed June 29, 2021, 2019.
- [20] Xu J, Hu J, Sun Y, Wang H, Wu Z, Hu J, Hochgreb S, Luo E. A cascade-looped thermoacoustic driven cryocooler with different-diameter resonance tubes. Part II: Experimental study and comparison. *Energy* 2020;207:118232.
- [21] Zhang L, Hu J, Wu Z, Luo E, Xu J, Bi T. A 1 kW-class multi-stage heat-driven thermoacoustic cryocooler system operating at liquefied natural gas temperature range. *Applied Physics Letters* 2015;107(3):033905.
- [22] Rayleigh JWSB. *The theory of sound*, vol. 2. Macmillan; 1896.

- [23] Offner A, Yang R, Felman D, Elkayam N, Agnon Y, Ramon GZ. Driven Acoustic Oscillations. by Boundary Mass Exchange, *Journal of Fluid Mechanics* 866 316–349. ISSN 2019;0022–1120:1469–7645.
- [24] Raspet R, Hickey CJ, Sabatier JM. The effect of evaporation-condensation on sound propagation in cylindrical tubes using the low reduced frequency approximation. *The Journal of the Acoustical Society of America* 1999;105(1):65–73.
- [25] Raspet R, Slaton WV, Hickey CJ, Hiller RA. Theory of inert gas-condensing vapor thermoacoustics: Propagation equation. *The Journal of the Acoustical Society of America* 2002;112(4):1414–22.
- [26] Tsuda K, Ueda Y. Abrupt reduction of the critical temperature difference of a thermoacoustic engine by adding water. *AIP Advances* 2015;5(9):097173.
- [27] Meir A, Offner A, Ramon GZ. Low-Temperature Energy Conversion Using a Phase-Change Acoustic Heat Engine. *Applied Energy* 231 2018;372–379. ISSN 03062619.
- [28] Yang R, Meir A, Ramon GZ. Theoretical Performance Characteristics of a Travelling-Wave Phase-Change Thermoacoustic Engine for Low-Grade Heat Recovery. *Applied Energy* 2020;261:114377.
- [29] Senga M, Hasegawa S. Energy conversion of thermoacoustic engines with evaporation and condensation. *International Journal of Heat and Mass Transfer* 2021;165:120385.
- [30] Slaton WV, Raspet R, Hickey CJ, Hiller RA. Theory of inert gas-condensing vapor thermoacoustics: Transport equations. *The Journal of the Acoustical Society of America* 2002;112(4):1423–30.
- [31] Yang R, Blanc N, Ramon GZ. Environmentally-sound: An acoustic-driven heat pump based on phase change. *Energy Conversion and Management* 2021;232: 113848.
- [32] Swift GW. Thermoacoustics A Unifying Perspective for Some Engines and Refrigerators, *Acoustical society of America* 2003.
- [33] Weltsch O, Offner A, Liberzon D, Ramon GZ, Streaming Adsorption-Mediated Mass. in a Standing Acoustic Wave, *Physical Review Letters* 118 (24), 244301. ISSN 2017;0031–9007:1079–7114.
- [34] Jin T, Yang R, Wang Y, Liu Y, Feng Y. Phase adjustment analysis and performance of a looped thermoacoustic prime mover with compliance/resistance tube. *Applied Energy* 2016;183:290–8.
- [35] Swift GW. Thermoacoustic engines. *The Journal of the Acoustical Society of America* 1988;84(4):1145–80.
- [36] Yazaki T, Iwata A, Maekawa T, Tominaga A. Traveling wave thermoacoustic engine in a looped tube. *Physical Review Letters* 1998;81(15):3128.
- [37] Gardner DL, Swift G. A cascade thermoacoustic engine. *The Journal of the Acoustical Society of America* 2003;114(4):1905–19.
- [38] Ceperley PH. A pistonless Stirling engine-The traveling wave heat engine. *The Journal of the Acoustical Society of America* 1979;66(5):1508–13.
- [39] Zajacs A, Bogdanovics R, Borodinacs A. Analysis of low temperature lift heat pump application in a district heating system for flue gas condenser efficiency improvement. *Sustainable Cities and Society* 2020;57:102130.